Available online at www.sciencedirect.com
SCIENCE DIRECT®
Journal of Power Sources 143 (2005) 231–235
JOURNAL OF POWER SOURCES
www.elsevier.com/locate/jpowsour

Short communication

Physicochemical and electrochemical characterization of anatase titanium dioxide nanoparticles

Zhaolin Liu*, Liang Hong, Bing Guo

Institute of Materials Research and Engineering, 3 Research Link, Singapore 117602, Singapore

Received 30 August 2004; accepted 24 November 2004
Available online 2 February 2005

Abstract

Nano-sized TiO_2 with an anatase phase is prepared by hydrolysis of titanium tetraisopropoxide in pure water. Samples are characterized by transmission electron microscopy (TEM), X-ray diffractometry (XRD) and X-ray photoelectron spectroscopy (XPS). TiO_2 nanoparticles experienced two processes of phase transition, i.e., amorphous to anatase and anatase to rutile, over the temperature range from 60 to 800 °C. The electrochemical properties of Li^+ ion insertion in nano-sized TiO_2 (anatase) electrodes is studied by voltammetry. The diffusion-limited insertion and extraction of Li ions in the anatase lattice within a region near the peak potential are dominating. The anatase TiO_2 nanoparticles exhibit a large initial electrochemical lithium insertion capacity of 195 mA h g^{-1}, good reversibility, and cyclic stability.

Keywords: Nano-sized TiO_2; Anatase; Electrochemical lithium insertion

1. Introduction

In recent years, lithium-ion intercalation materials have been examined for the development of cheap and efficient lithium-ion batteries. Nanostructured TiO_2 is an interesting candidate for 2-V lithium-ion batteries due to its convenient formal potential of around 1.8 V (versus Li/Li^+) [1–3]. TiO_2 has various crystal types, such as rutile, anatase, brookite, and ramsdellite-type $Li_2Ti_3O_7$, spinels [4,5]. The lithium insertion reaction into these hosts has been investigated [6–8]. The Li uptake has been found to be 0.5 in anatase, whereas only a weak intercalation of Li has been detectable for rutile cells. Stashans et al. [9] studied lithium insertion into anatase and rutile by quantum chemical Hartree-Fock calculations. The results predicted a higher possibility of lithium intercalation in the anatase structure than that in rutile. The ability of the anatase phase to intercalate a large number of Li-ions makes it a good candidate for application in high density, 2-V, lithium-ion batteries.

The present work focus on the synthesis and assessment of nano-sized TiO_2 prepared by a sol-gel method from a precursor of $Ti[OCH(CH_3)_2]_4$. Enhanced electrochemical lithium insertion capacity together with good reversibility and cyclic stability are demonstrated.

2. Experimental

2.1. Preparation of TiO_2 nanoparticles

A solution of 30 mL of titanium tetraisopropoxide ($Ti[OCH(CH_3)_2]_4$, Aldrich, A.C.S. Reagent) and 5 mL of isopropyl alcohol was added dropwise (1 mL min^{-1}) into 180 mL of distilled water at pH 1.5 (adjusted with HNO_3). The resulting solution was continuously stirred for 10 to 12 h until a transparent colloid was formed. The colloid solution was concentrated at 60 °C with a rotary evaporator

* Corresponding author. Fax: +65 68720785.
E-mail address: zl-liu@imre.a-star.edu.sg (Z. Liu).

0378-7753/$ – see front matter © 2004 Elsevier B.V. All rights reserved.
doi:10.1016/j.jpowsour.2004.11.056

and then calcined at 600 to 800 °C for 2 h in air to yield TiO_2 nanoparticles.

2.2. Characterization

The size and morphology of TiO_2 composites were characterized by transmission electron microscopy (TEM) imaging (JEOL JEM 2010). Samples were first ultrasonicated in acetone for 1 h and then deposited on 3-mm copper grids that were covered with a continuous film of carbon. Crystalline structures of the powders were characterized by X-ray diffraction (XRD) with a Bruker GADDS diffractometer using Cu Kα radiation and a graphite monochromator (the accelerating voltage and the applied current were 40 kV and 40 mA, respectively). X-ray photoelectron spectroscopy (XPS) analysis of the samples was performed by means of a VG ESCALAB MKII spectrometer. Narrow-scan photoelectron spectra of Ti 2p and O 1s were recorded. Peak deconvolution was performed using the curve-fitting program VGX900.

2.3. Electrochemical lithium insertion

TiO_2 was mixed with 10 wt.% of carbon black and 10 wt.% of poly vinylidene difluoride (PVDF) in 1-methyl-2-pyrrolidone (NMP). The slurry was used to coat 20-μm thick aluminium discs of 13 mm diameter to a mass loading of 2 mg cm^{-2} after drying (at 120 °C) and compaction (at 2.0×10^6 Pa). Each coated electrode was assembled in a 2016 coin cell using a lithium counter electrode, a microporous polypropylene separator, and an electrolyte of 1 M $LiPF_6$ in a 50:50 (w/w) mixture of ethylene carbonate (EC) and diethyl carbonate (DEC). Cell assembly was carried out in an argon-filled glove box with less than 1 ppm each of oxygen and moisture.

The cells were discharged and charged at 25 °C on a MACCOR battery test system. Cyclic voltammetry was conducted with a EG&G model 273 potentiostat/galvonostat.

3. Results and discussion

The results of thermal analysis of TiO_2 xerogels that record the weight loss and DTA profiles of each sample with temperature are presented in Fig. 1. The total weight loss value was about 24% and profile was flat after 400 °C, which indicated that organic residues were eliminated before this temperature. The DTA profiles of TiO_2 xerogels exhibit a three-step weight loss. The weight loss below 100 °C corresponds to the removal of adsorbed isopropyl alcohol. The second weight loss at about 110 °C is attributed to the removal of adsorbed water. The third weight loss, between 190 and 400 °C, is attributed to the expulsion of organics and the removal of structural hydroxyls, which increases the number of bridging oxygen atoms and thus the monolithic nature of the gel matrix [10].

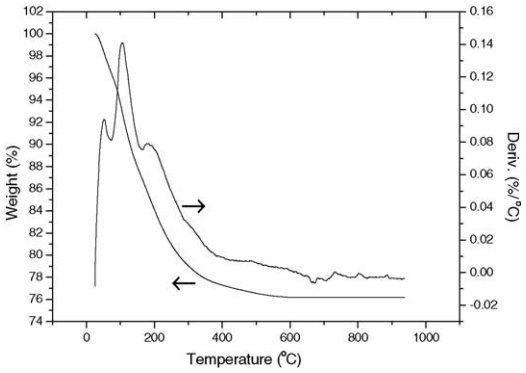

Fig. 1. TG and DTA traces for TiO_2 xerogels.

To determine the actual sizes of the powder samples, the TiO_2 powder calcined at 600 °C was suspended in ethanol under sonification for 1 h. The results, as shown in Fig. 2, indicate that the powder is highly aggregated. The average particle size of the individual particles is about 20 nm or less and it seems that most of the fine particles are round in shape.

X-ray diffraction analysis was used to identify the crystal phases, to estimate the anatase to rutile ratio, and to determine the crystallite size of each phase present. The TiO_2 exists mainly in three crystallographic forms, namely: anatase, brookite and rutile. The rutile form is thermodynamically more stable than the anatase counterpart. Brookite is the unstable phase of TiO_2. The XRD peaks at $2\theta = 25.25$ (101) and 48.0° in the spectrum for TiO_2 are easily identified as the anatase form, whereas the peaks at $2\theta = 27.42$ (110) and 54.5° belong to the rutile form. The XRD patterns of the as-prepared gel powder of TiO_2 and the powders calcined at different temperatures are given in Fig. 3. All the peaks for gel powder show the presence of both anatase and amorphous phases. With increasing calcination temperature, the intensity of the anatase peaks increased correspondingly. The average crystallite size (diameter) L can be estimated from the integral width of the diffraction peaks using the Scherrer formula: $L = K\lambda/\beta \cos\theta$, where K is the shape factor (a value of 0.9 was used in this study), λ is the X-ray radia-

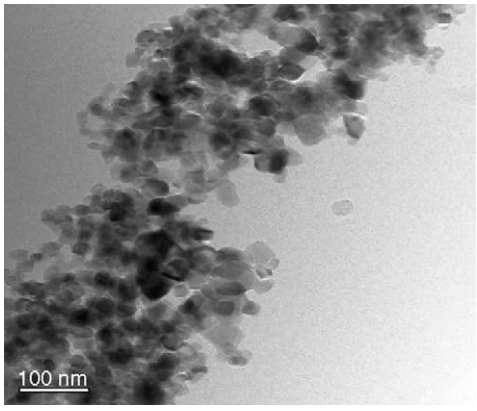

Fig. 2. TEM image of TiO_2 powder calcined at 600 °C and suspended in ethanol under sonification for 1 h.

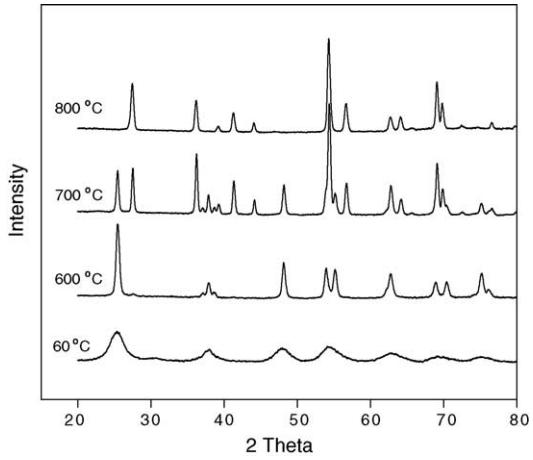

Fig. 3. XRD patterns of as-prepared gel powder of TiO_2 and powders calcined at different temperatures.

tion wavelength (1.54056 Å for Cu Kα), and β is the line width at half-maximum height of the main broadening. The calculation results, which are 7.8, 18.5 and 22.7 nm for pure TiO_2 calcined at 60, 600 and 700 °C, respectively, indicate that the average crystalline size of the resulting anatase phase increases with increasing calcination temperature.

Several studies [11–15] have reported that a sol-gel sample of TiO_2 should undergo a phase transformation from an anatase phase to a thermodynamically favourable rutile phase during sintering treatment. In the present study, all the samples were sintered from 400 to 800 °C and their diffractograms were recorded. It is observed that TiO_2 undergoes the phase transformation somewhat above 600 °C. The conversion of TiO_2 from anatase to rutile is thorough, almost no anatase peak can be observed after sintering at 800 °C.

The surface oxidation states of the metals were determined by XPS. As most of the atoms in small particle clusters are surface atoms, the oxidation state measured as such will also reflect well the bulk oxidation state. The Ti 2p and O 1s regions of the XPS spectrum for the TiO_2 are shown in Fig. 4. In the XPS spectrum for Ti 2p, the spin-orbit components ($2p_{3/2}$ and $2p_{1/2}$) of the peak are well deconvoluted by two curves (at approximately 458.7 and 464.3 eV, respectively). This indicates that the Ti element exists mainly as the chemical state of Ti^{4+} on the basis of the principle and instrument handbook of XPS [16]. The two eV values agree well with those reported in the literature [17,18].

The XPS spectra of O 1s in Fig. 4 is asymmetric, i.e., the left side is wider than the right, and this indicates that at least two kinds of oxygen species are present on the surface, which can be recognized by resolving the XPS curves. The dominant peak at about 530 eV is characteristic of metallic oxides, which is in agreement with the O 1s electron binding energy arising from titania lattice. The oxygen atoms in the titania matrix make the primary contribution to the spectrum. The other O 1s peak at 532 eV is due to surface hydroxyl groups.

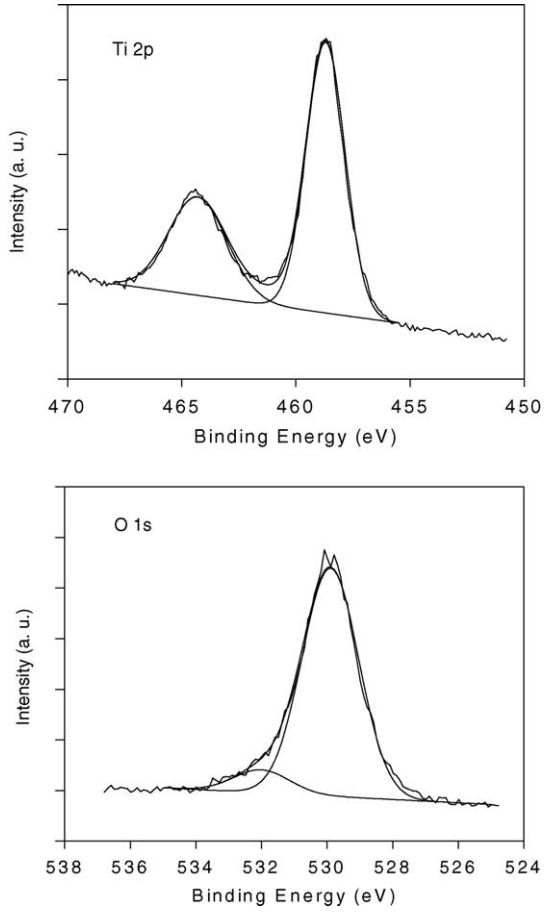

Fig. 4. Typical XPS Ti 2p and O 1s spectra for TiO_2 sample calcined at 600 °C.

The discharge–charge curves of the electrode made of anatase TiO_2 nanoparticles are shown in Fig. 5. The initial discharge and charge capacity of the electrode is 203 and 177 mA h g^{-1}, respectively, which indicates an initial loss in capacity of about 14% between the insertion and the removal

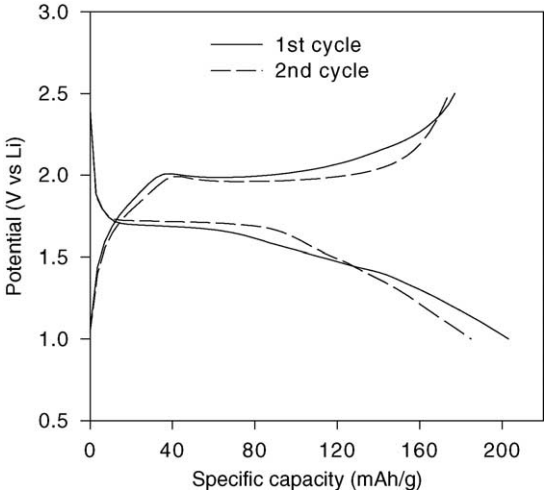

Fig. 5. Charge and discharge curves for nano-sized anatase TiO_2 electrode at charge–discharge current density of 50 mA g^{-1} at 25 °C.

of Li. The loss in capacity for the second discharge–charge cycle decreases to 6% between insertion and removal of Li. Potential plateaux at about 1.72 and 2.00 V for discharging (insertion of Li) and charging (extraction of Li) are observed, which is consistent with the presence of predominantly anatase TiO_2 [2,19]. Thus, the electrochemical behaviour is assigned to the insertion/extraction of Li to/from the anatase lattice:

$$TiO_2 + x(Li^+ + e^-) \rightarrow Li_xTiO_2 \quad (1)$$

Theoretically, insertion of 1 Li per TiO_2 unit corresponds to a capacity of 335 mA h g^{-1}. The insertion coefficient, x, in anatase is usually close to 0.5 [20]. The maximum extraction coefficient of lithium in TiO_2 nanoparticles is calculated to be 0.53 from an electrochemical charge capacity of 177 mA h g^{-1}. The interaction of the nanoparticles with lithium ions occurs mostly on the surface rather than in the bulk due to the small particle size. This means that lithium insertion/extraction can be readily achieved in TiO_2 nanoparticles. This will result in a higher storage capacity with respect to ordinary anatase TiO_2.

The cyclic voltammograms of the electrode made of the anatase TiO_2 nanoparticles at different scan rates are shown in Fig. 6. A pair of cathodic (insertion) and anodic (extraction) peaks located between 1.4 and 2.5 V are observed. The actual peak positions depend on the applied scan rate. If the capacitive effects are neglected, dependence of the peak current, i_p on the square root of the scan rate, ν indicates a diffusion-controlled irreversible kinetics [21,22], i.e.,

$$|i_p| = 0.4958\, nFAC\left(\frac{D\alpha n F\nu}{RT}\right)^{1/2} \quad (2)$$

where: i_p is the peak current in amperes; n is taken as unity; A is the inner electrode area in cm^2; C is the maximum obtainable concentration of Ti^{3+} in the lattice, i.e., $C = 0.024$ mol cm^{-3} for $x = 0.5$ [22]; D is the chemical diffusion constant for the Li ions in $cm^2\ s^{-1}$; the other symbols

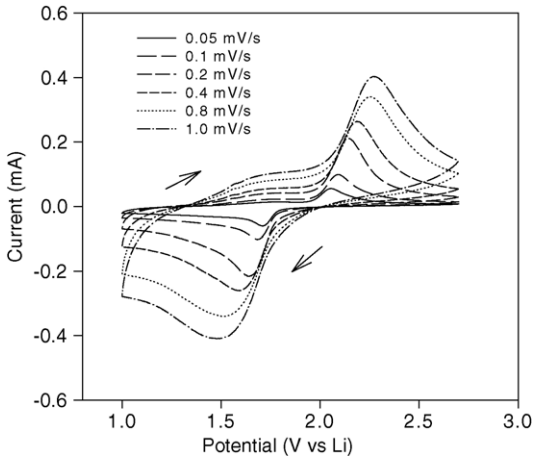

Fig. 6. Cyclic voltammograms for nano-sized anatase TiO_2 electrode at various scan rates.

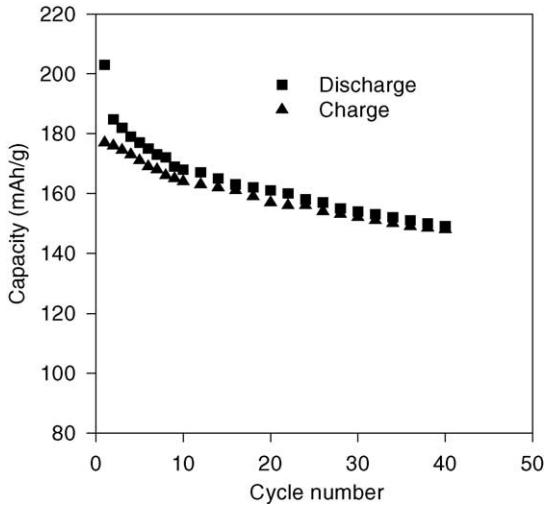

Fig. 7. Dependence of cyclability of nano-sized anatase TiO_2 electrode at charge–discharge current density of 50 mA g^{-1} at 25 °C.

have their usual meaning. Even if the capacitive charging cannot be neglected, the i_p–ν dependency (for anatase) still follows a power-law with the exponent of ν being between 0.5 and 1 [22]. The cathodic and anodic peaks scales are dependent upon $\nu^{1/2}$ for scan rates between 0.05 and 1 mV s^{-1}. Assuming $\alpha \approx 0.5$ and a roughness factor of 80, the diffusion coefficient can be calculated from Eq. (2) for cathodic and anodic peaks. The values for insertion and extraction are 2.9×10^{-17} and 3.7×10^{-17} $cm^2\ s^{-1}$, respectively. The values agree with those reported for nanoporous anatase TiO_2 electrodes [23].

The discharge–charge behaviour of the electrode made of anatase TiO_2 nanoparticles at 50 mA g^{-1} is demonstrated in Fig. 7. The cut-off potentials for discharge and charge were set to be 1.0 and 2.5 V versus Li, respectively. The electrode shows good stability towards electrochemical cycling. The reversible capacity after 40 cycles is 148 mA h g^{-1}, or 84% retention of initial capacity. Progressive lithium insertion in TiO_2 anatase leads to an increase in the fraction lithium titanate phase and a decrease in the lithium anatase phase fraction [19]. The optimum cycling behaviour is obtained for regimes that involve compositions between 0.15 and 0.45 Li/TiO_2 mole ratio, as reported previously [1]. It is very necessary to improve the stability of the TiO_2 electrode.

4. Conclusions

Anatase TiO_2 nanoparticles with a particle size of about 20 nm are prepared by hydrolysis of titanium tetraisopropoxide in pure water. X-ray diffraction analysis reveals that TiO_2 nanoparticles experience two processes of phase transition, i.e., amorphous to anatase and anatase to rutile, over the temperature range from 60 to 800 °C. Cyclic voltammetry measurements indicate that the diffusion-limited insertion and extraction of Li^+ ions in the anatase lattice within a region

near the peak potential are dominating and yield diffusion coefficients of the order of 10^{-17} cm^2 s^{-1}. The anatase TiO_2 nanoparticles exhibit a large initial electrochemical lithium insertion capacity of 203 mA h g^{-1}, as well as, good reversibility and cyclic stability.

References

[1] F. Bonino, L. Busani, M. Lazzari, M. Anstretta, B. Rivolta, B. Scrosati, J. Power Sources 6 (1981) 261.
[2] S.Y. Huang, L. Kavan, I. Exnar, M. Gratzel, J. Electrochem. Soc. 142 (1995) L142.
[3] O. Wilhelm, S.E. Pratsinis, E. de Chambrier, M. Crouzet, I. Exnar, J. Power Sources 134 (2004) 197.
[4] J.F. Banfield, D.R. Veblen, Am. Miner. 77 (1992) 545.
[5] T. Ebina, T. Iwasaki, Y. Onodera, H. Hayashi, T. Nagase, A. Chatterjee, K. Chiba, J. Power Sources 81–82 (1999) 393.
[6] S. Garnier, C. Bohnke, O. Bohnke, J.L. Fourquet, Solid State Ionics 83 (1996) 323.
[7] B. Zachau-Christiansen, K. West, T. Jacobsen, S. Atlung, Solid State Ionics 40–41 (1990) 580.
[8] B. Zachau-Christiansen, K. West, T. Jacobsen, S. Skaarup, Solid State Ionics 53–56 (1992) 364.
[9] A. Stashans, S. Lunell, R. Bergström, A. Hagfeldt, S.E. Lindquist, Phys. Rev. B 53 (1996) 150.
[10] C.P. Sibu, S. Rajesh Kumar, P. Mukundan, K.G.K. Warrier, Chem. Mater. 14 (2002) 2876.
[11] H. Zhang, J.F. Banfield, J. Phys. Chem. B. 104 (2000) 3481.
[12] J. Ovenstone, K. Yanagisawa, Chem. Mater. 11 (1999) 2770.
[13] S.J. Kim, S.D. Park, Y.H. Jeong, J. Am. Ceram. Soc. 82 (1999) 927.
[14] B.R. Reddy, A. Khan, Y. Yamada, T. Kobayashi, S. Loridant, J. Volta, J. Phys. Chem. B 107 (2003) 5162.
[15] J. Lin, J.C. Yu, J. Photochem. Photobiol. A 116 (1998) 63.
[16] N.M. Rahman, K.M. Krishna, T. Soga, T. Jimbo, M. Umeno, J. Phys. Chem. Solids 60 (1999) 201.
[17] L. Biener, M. Baumer, J. Wang, R.J. Madrix, Surf. Sci. 450 (2000) 12.
[18] Q. Wang, R.J. Madrix, Surf. Sci. 474 (2001) L213.
[19] X. Gao, H. Zhu, G. Pan, S. Ye, Y. Lan, F. Wu, D. Song, J. Phys. Chem. B 108 (2004) 2868.
[20] L. Kavan, M. Grätzel, J. Rathousky, A. Zukal, J. Electrochem. Soc. 143 (1996) 394.
[21] R. Van de Krol, A. Goossens, J. Schoonman, J. Phys. Chem. B 103 (1999) 7151.
[22] H. Lindström, S. Södergen, A. Solbrand, H. Rensmo, J. Hjelm, A. Hagfeldt, S.E. Lindquist, J. Phys. Chem. B 101 (1997) 7717.
[23] L. Kavan, J. Rathousky, M. Grätzel, V. Shklover, A. Zukal, J. Phys. Chem. B 104 (2000) 12012.